EurJIC European Journal of Inorganic Chemistry

DOI: 10.1002/ejic.201101193

Synthesis of Uniformly Sized Manganese Oxide Nanocrystals with Various Sizes and Shapes and Characterization of Their T_1 Magnetic Resonance Relaxivity

Kwangjin An,[a] Mihyun Park,[a] Jung Ho Yu,[a] Hyon Bin Na,[a] Nohyun Lee,[a] Jongnam Park,[a,b] Seung Hong Choi,[c] In Chan Song,[c] Woo Kyung Moon,[c] and Taeghwan Hyeon*[a]

Keywords: Manganese / Nanoparticles / Thermal decomposition / Heat-up process / Imaging agents

We synthesized manganese oxide (MnO and Mn_3O_4) nanocrystals with various sizes and shapes by the thermal reaction of a Mn^{II}–oleate complex through a "heat-up process". When a Mn^{II}–oleate complex was thermally decomposed in non-coordinating hydrocarbon solvents, uniformly sized MnO nanocrystals with cubic and octahedral shapes were produced. We were able to synthesize anisotropic, multi-branched MnO nanocrystals by the oriented attachment of MnO truncated-nanocube building blocks. When the Mn^{II}–oleate complex was heated in 1-hexadecene in the presence of strongly coordinating carboxylic acid surfactants, spherical nanocrystals were generated, and their diameter was controlled in the range 3–13 nm by varying the chain length of the carboxylic acid. When oleyl alcohol was added to the Mn–oleate complex in phenyl ether, tetrahedral MnO nanocrystals were synthesized. The as-synthesized MnO nanocrystals were oxidized in air to Mn_3O_4 or MnO/Mn_3O_4 core–shell structures, which exhibited exchange coupling with shifted magnetic hysteresis loops. The effect of the size and shape of the phospholipid-capped manganese oxide nanocrystals on their applicability as T_1 contrast agents in magnetic resonance imaging (MRI) were examined. As the size of the nanocrystals decreased, their relaxivities increased, thereby generating brighter MR images. In particular, spherical 3 nm-sized Mn_3O_4 nanocrystals had a high specific relaxivity (r_1) of 2.38 $mM^{-1}s^{-1}$, clearly demonstrating their potential for use as an efficient T_1 MRI contrast agent.

Introduction

The designed synthesis of uniformly sized nanocrystals with controlled sizes and shapes is of great importance for both fundamental science and technical applications, because the properties of nanocrystals directly depend on their size and shape.[1] Recently, manganese oxide nanocrystals have attracted a lot of attention because of their unique magnetic properties, which result from both the variable oxidation states of their manganese ions (Mn^{2+}, Mn^{3+}, and Mn^{4+}) and their high surface-to-volume ratio.[2] Recent reports demonstrated that MnO nanocrystals were readily oxidized to MnO/Mn_3O_4 core–shell structures, which exhibit exchange coupling at the interface of two magnetic components.[3] Various methods have been reported for the synthesis of manganese oxide nanocrystals with various sizes and shapes.[4] In particular, thermal decomposition of metal–oleate complexes through a "heat-up process" has been used to produce uniformly sized manganese oxide nanocrystals.[5,6]

A tremendous amount of research has been performed on the applications of magnetic iron oxide nanocrystals as T_2 contrast agents in magnetic resonance imaging (MRI).[7] On the other hand, biocompatible manganese oxide nanocrystals have been developed as new T_1 MRI contrast agents for in vivo diagnosis.[8] However, there have been very few reports on the size- and shape-dependent T_1 contrast properties of manganese oxide nanocrystals.[9] Herein, we report on the size- and shape-controlled synthesis of manganese oxide nanocrystals by thermal decomposition of a Mn–oleate complex through a heat-up process. Various manganese oxide nanocrystals were synthesized, having not only thermodynamically controlled cubic, octahedral, and spherical shapes but also kinetically controlled branched or tetrahedral shapes. Crystal structures as well as size- and shape-dependent magnetic properties of the synthesized manganese oxide nanocrystals were determined. Furthermore, we investigated the T_1 relaxation properties of the

[a] World Class University (WCU) Program of Chemical Convergence for Energy & Environment (C2E2), Institute of Chemical Processes, and School of Chemical and Biological Engineering, Seoul National University, Seoul 151-744, Korea
E-mail: thyeon@snu.ac.kr
[b] Interdisciplinary School of Green Energy, School of Nano-Bioscience and Chemical Engineering, Ulsan National Institute of Science and Technology (UNIST), Ulsan 681-800, Korea
[c] Department of Radiology, Seoul National University College of Medicine, Seoul National University Hospital, Seoul 110-744, Korea

Supporting information for this article is available on the WWW under http://dx.doi.org/10.1002/ejic.201101193.

manganese oxide nanocrystals dispersed in water with regard to their potential applications as MRI contrast agents.

Results and Discussion

Uniformly sized MnO nanocrystals with cubic and octahedral shapes were synthesized by the thermal decomposition of a Mn^{II}–oleate complex in non-coordinating hydrocarbon solvents. When a solution of the Mn^{II}–oleate complex in 1-hexadecene was slowly heated to reflux (288 °C), without the employment of any additional surfactant, and kept at that temperature for 1 h, uniformly sized MnO nanocubes with an edge length of 16 nm were synthesized (Figure 1a). When the reaction was conducted in 1-octadecene instead of 1-hexadecene at a higher temperature of 320 °C for 30 min, octahedral MnO nanocrystals with an average edge length of 26 nm were generated (Figure 1b). When the synthesis was conducted for a longer time of 1 h, the edge length of the octahedral nanocrystals increased slightly to 29 nm (Figure 1c). In the heat-up process, traces of water and oxygen significantly affect not only the crystallinity and phase of the manganese oxide nanocrystals[4c,10] but also the uniformity of their size and shape.[6] Therefore, the Mn^{II}–oleate complex was completely dried under vacuum to yield a pink powder (Supporting Information Figure S1), and the synthesis was performed using standard Schlenk techniques. The X-ray diffraction (XRD) pattern revealed that the as-synthesized MnO nanocrystals possess a cubic rock-salt structure ($Fm\bar{3}m$, JCPDS No. 78–0424) without any contamination by Mn_3O_4 (Supporting Information, Figure S3).[4] Because of the extremely narrow size distribution of the nanocrystals, 2D superlattices were readily generated. Furthermore, the superlattice structure depended on the shape of the MnO nanocrystals.[11] For example, the cubic MnO nanocrystals assembled to form a rectangular structure (Figure 1a), while the octahedral MnO nanocrystals were hexagonally assembled (Figure 1b and c). Under the current thermal decomposition reaction conditions, the relatively small nanocrystals (of size less than 16 nm) synthesized at low temperature were preferentially cubic, while the large nanocrystals with diameters greater than 20 nm, which were synthesized at a high temperature of 320 °C, were octahedral. In a cubic rock-salt structure, the three low-energy surfaces are the {100}, {110}, and {111} crystal planes, with a surface-energy ratio of 1/1.41/1.73.[12] Therefore, we speculate that at relatively low temperatures, the smaller and {100}-surface-developed cubes formed to minimize the total surface energy, while at high temperatures the larger and {111}-surface-developed nano-octahedrons could be generated, as high temperatures provide sufficient energy for nanocrystals to grow along the {100} surface. Furthermore, the formation mechanism for MnO nanocubes is very similar to that of 5 nm-sized iron oxide nanocubes.[5a]

When strongly coordinating carboxylic acid surfactants with long hydrocarbon chains were added to the reaction mixture, spherical nanocrystals were generated (Figure 2). The particle size was controlled by varying the chain length of the carboxylic acids. For example, spherical MnO nanocrystals with particle diameters of 3 nm (Figure 2a), 5 nm (Figure 2b), 11 nm (Figure 2c), and 13 nm (Figure 2d) were synthesized by using behenic acid ($C_{21}H_{43}COOH$), stearic acid ($C_{17}H_{35}COOH$), myristic acid ($C_{13}H_{27}COOH$), and decanoic acid ($C_9H_{19}COOH$), respectively. In view of the average surface energy of a rock-salt-structured sphere, which is between the surface energy of nanocubes and nano-octahedrons, the experimental results show that, regardless of the nanocrystal size, excess carboxylic acid surfactant further reduces the surface energy, inhibiting shape-controlled growth and resulting in the formation of spherical nanocrystals.[13] The XRD patterns reveal that the as-synthesized MnO nanocrystals with sizes of 11 and 13 nm have a pure cubic rock-salt crystal structure (JCPDS No. 78-0424), whereas the nanocrystals with sizes of 3 and 5 nm possess mixed crystal structures of cubic MnO and tetragonal Mn_3O_4 (JCPDS No. 80–0382) (see Supporting Information, Figure S4). It seems that the small MnO nanocrystals with a high surface-to-volume ratio are readily oxidized in air. Recent studies demonstrated that the as-synthesized MnO nanocrystals were transformed to MnO/Mn_3O_4 core–shell structures by surface oxidation in air, resulting in the formation of exchange-coupled magnetic structures with shifted magnetic hysteresis loops.[3] On the other hand, when we intentionally oxidized the 26 nm-sized MnO nanocrystals by using trimethylamine *N*-oxide as an oxidant, pure Mn_3O_4 nanocrystals were generated (Supporting In-

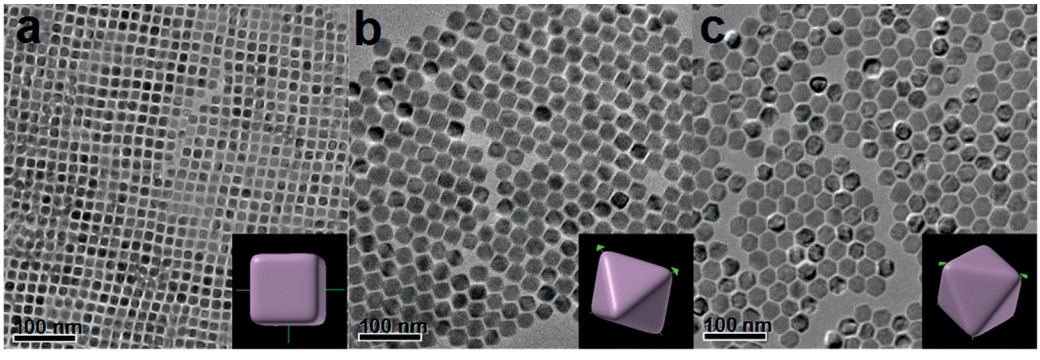

Figure 1. TEM images of MnO nanocrystals with (a) cubic and (b,c) octahedral shapes. The mean lengths of their edges are (a) 16 nm, (b) 26 nm, and (c) 29 nm.

formation, Figure S5).[4a,4e] The result implies that Mn_3O_4 nanocrystals with various sizes and shapes could be synthesized by further oxidation of as-synthesized MnO nanocrystals.

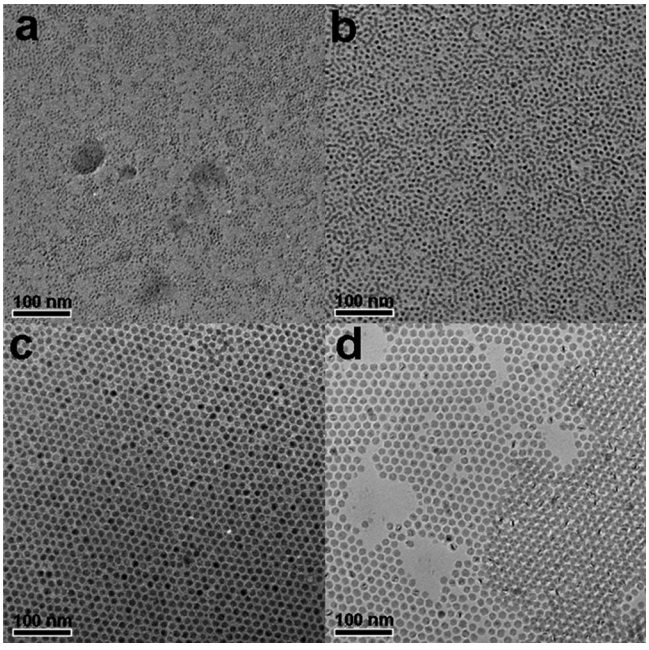

Figure 2. TEM images of spherical MnO nanocrystals with nanocrystal diameters of (a) 3 nm, (b) 5 nm, (c) 11 nm, and (d) 13 nm, synthesized by using behenic acid, stearic acid, myristic acid, and decanoic acid, respectively.

As described above, when the Mn–oleate complex was heated to reflux in non-coordinating solvents, such as 1-hexadecene (288 °C) and 1-octadecene (320 °C), isotropic MnO nanocrystals with cubic and octahedral shapes were generated. However, when the Mn–oleate complex was heated at a slightly lower temperature of 280 °C in the presence of excess carboxylic acid surfactants, club-shaped MnO nanorods were produced. For example, when myristic acid was used as the carboxylic acid surfactant, MnO nanorods with club-shaped tips at both ends were generated (Figure 3a), whereas a mixture of club-shaped nanorods and T-shaped nanorods with club-shaped tips at all extremities was produced when decanoic acid was used in the synthesis (Figure 3b). It is interesting that this little difference in the reaction temperature completely changed the final shape of the nanocrystals.[14] Furthermore, when we performed the synthesis at an intermediate temperature of 285 °C, a mixture of spherical and rod-shaped MnO nanocrystals was generated (Figure 3c). The high-resolution transmission electron microscopy (HRTEM) image of a MnO nanorod revealed that truncated nanocubes of approximately 10 nm in size with a {200} crystal lattice parameter of 2.17 Å were aligned along the <100> direction (Figure 3d). From these results, we concluded that the anisotropic growth of MnO nanocrystals proceeded by the oriented attachment mechanism.[15,16]

The addition of alcohol during the heat-up process is known to significantly alter the nanocrystal growth behav-

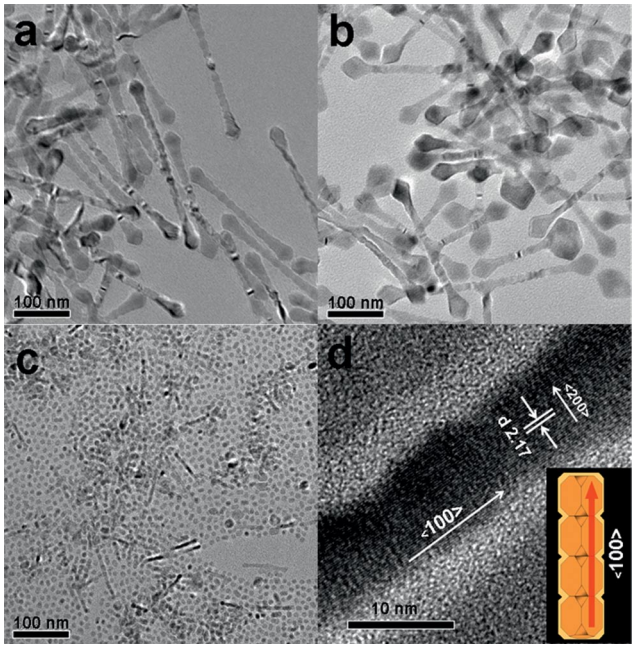

Figure 3. TEM images of (a) rod-shaped and (b) T-shaped MnO nanocrystals and of (c) a mixture of spherical MnO nanocrystals and anisotropic MnO nanocrystals. (d) High-resolution TEM image of rod-shaped MnO nanocrystals (inset: schematic illustration showing the oriented attachment of the MnO nanocrystals along the <100> direction).

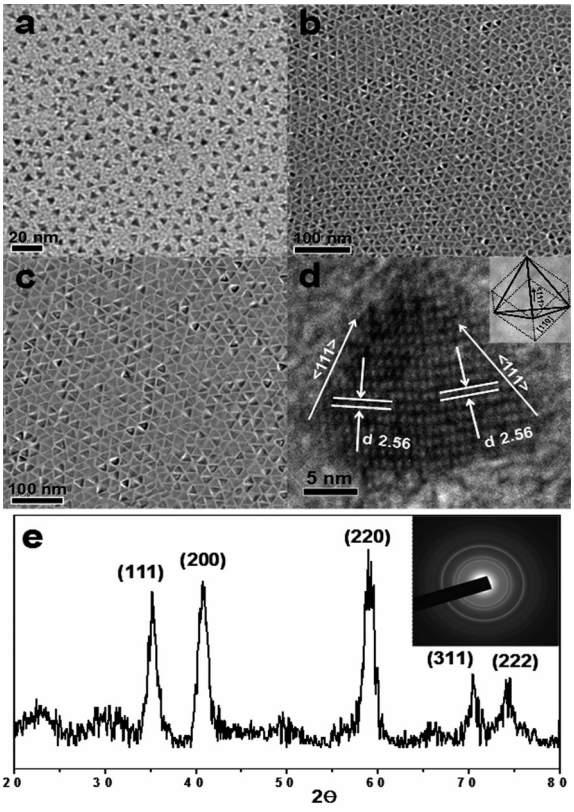

Figure 4. TEM images of tetrahedral MnO nanocrystals with lateral dimensions of (a) 6 nm, (b) 8 nm, and (c) 20 nm. (d) HRTEM image and (e) XRD pattern of 20 nm-sized nanocrystals.

ior.[17] When oleyl alcohol was injected into a Mn–oleate solution in phenyl ether solvent at 260 °C, tetrahedral MnO nanocrystals were obtained (Figures 4 and S6). By controlling the heating rate and the reaction time, the edge length of the tetrahedral nanocrystals was adjusted to 6, 8, and 20 nm (Figures 4a, b, and c, respectively). The HRTEM image (Figure 4d) and XRD pattern (Figure 4e) clearly show that the tetrahedral MnO nanocrystals possess a cubic rock-salt crystal structure.[4] The well-defined lattice planes with their interplanar distance of 2.56 Å show that tetrahedral MnO nanocrystals were generated with the development of the {110} surface, which has the second lowest surface energy in a cubic rock-salt structure.[12] Considering that the growth temperature of tetrahedral MnO nanocrystals (260 °C) is significantly lower than that of {100}-surface-developed cubic (288 °C) or {111}-surface-developed octahedral (320 °C) nanocrystals, we speculate that the oleyl alcohol coordinates on the nanocrystal surface to lower the surface energy, consequently altering the nanocrystal growth behavior. Furthermore, in the formation of the tetrahedral MnO nanocrystals, not only oleyl alcohol but also the ether played an important role. While phenyl ether could be replaced with octyl ether for the synthesis of tetrahedral MnO nanocrystals, the addition of a non-coordinating solvent, such as 1-octadecene, instead of phenyl ether, resulted in the formation of octahedral MnO nanocrystals (Supporting Information, Figure S7). To the best of our knowledge, this is the first report on the synthesis of tetrahedral MnO nanocrystals. The experimental conditions used for the preparation of the various manganese oxide nanocrystals and the size distribution histograms described above are summarized in Table S1 and Figure S8 of the Supporting Information.

We investigated the size-dependent magnetic properties of spherical and tetrahedral manganese oxide nanocrystals. The temperature dependence of the magnetization of manganese oxide nanocrystals was measured with zero-field-cooling (ZFC) and field-cooling (FC) procedures in an applied magnetic field of 100 Oe in the temperature range 5–300 K (Figure 5a, b).[18] The observed blocking temperatures (T_B) were 15, 17, 17, and 24 K for spherical nanocrystals with diameters of 3, 5, 11, and 13 nm, respectively, and 24, 31, and 24 K for tetrahedral nanocrystals with edge lengths of 6, 8, and 20 nm, respectively. When MnO nanocrystals are exposed to air, they are spontaneously oxidized to core–shell structured MnO/Mn_3O_4 mixtures or Mn_3O_4.[3] The degree of surface oxidation varies with nanocrystal size and shape. In the case of spherical nanocrystals, MnO nanocrystals with sizes of 3 and 5 nm were fully transformed to Mn_3O_4 (Supporting Information, Figure S9).

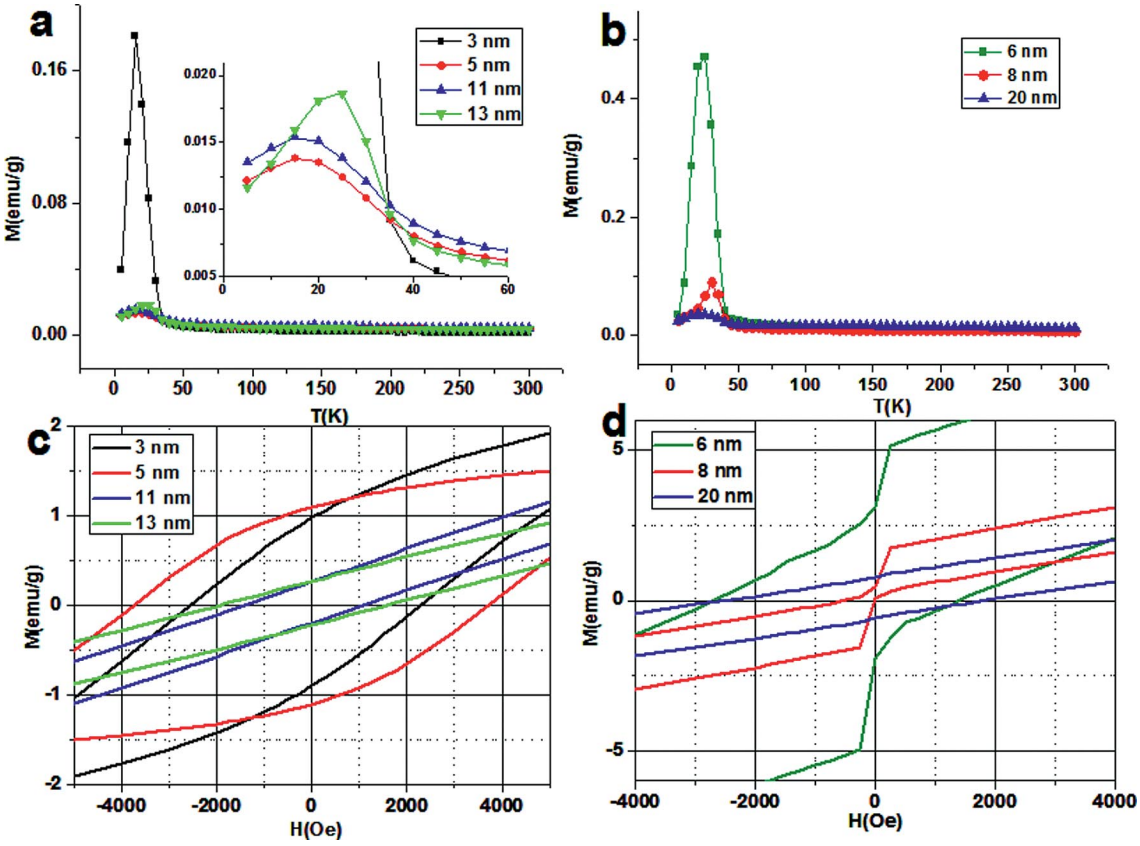

Figure 5. (a,b) Temperature and (c,d) field dependence of magnetizations of (a, c) spherical and (b, d) tetrahedral manganese oxide nanocrystals, which were stored under ambient conditions for one month. [All of the magnetization measurements were carried out at the temperature range 5–300 K, after zero-field cooling (ZFC) or field cooling (FC) with an applied field of 100 Oe from 300 K, and magnetic hysteresis loops were measured at 5 K.].

The blocking temperatures of the spherical Mn_3O_4 nanocrystals of size 3 and 5 nm have a linear relationship with their particle volume, which is consistent with previous reports.[4a–4c] However, the nanocrystals of size 11 and 13 nm were transformed to a MnO/Mn_3O_4 core–shell structure. The core–shell structure is composed of an antiferromagnetic core and a ferrimagnetic shell, and the structure is known to exhibit exchange bias, that is, a displacement of the hysteresis loop along the magnetic field axis.[19] As shown in Figure 5c, spherical MnO/Mn_3O_4 core–shell nanocrystals with sizes of 11 and 13 nm exhibit high exchange bias with 250 Oe of exchange bias field (H_E), while spherical Mn_3O_4 nanocrystals of size 3 and 5 nm exhibit negligible exchange bias (Supporting Information, Table S2). Likewise, the tetrahedral MnO nanocrystals with sizes of 6 and 8 nm were transformed to MnO/Mn_3O_4 core–shell structures, which exhibited exchange bias with 700 and 300 Oe of H_E, respectively (Figure 5d). On the other hand, air-oxidation of tetrahedral 20 nm-sized MnO nanocrystals was not detected by X-ray diffraction. Consequently, the blocking temperature of the tetrahedral 20 nm-sized MnO nanocrystals was slightly lower than that of the smaller MnO/Mn_3O_4 core–shell structured nanocrystals. Furthermore, the tetrahedral nanocrystals with edge lengths of 6 and 8 nm show an anomalous hysteresis with steps, which is presumably due to the exchange bias combined with the unique morphology of tetrahedral MnO/Mn_3O_4 core–shell structures (Figure 5d).[20] The experimental results show that the magnetic properties of manganese oxide nanocrystals strongly depend on their detailed crystalline structures.

Recently, biocompatible MnO nanocrystals were proposed as a new T_1 MRI contrast agent, and their size-dependent T_1 relaxation properties were characterized.[8] The smaller MnO nanocrystals exhibited brighter signal enhancement in the T_1-weighted MRI than the larger ones.[8a] Later, it was reported that as-synthesized MnO nanocrystals were spontaneously oxidized to Mn_3O_4 nanocrystals in air.[9a] The T_1 relaxation property of as-synthesized Mn_3O_4 nanocrystals was reported to be due to Mn^{2+} ions on the surface of Mn_3O_4.[9,21] In this study the size of the manganese oxide nanocrystals could be maintained in a smaller size regime more readily, relative to the previous study. Therefore, measurements of the T_1 and T_2 relaxation times of water dispersions of spherical Mn_3O_4 nanocrystals with particle sizes of 3, 5, 11, and 13 nm were performed with a 1.5 T clinical MRI scanner. Figure 6a shows the T_1-weighted images and their specific relaxivities (r_1 and r_2) measured at various nanocrystal concentrations. As the size of the Mn_3O_4 nanocrystals decreased, the specific relaxivity (r_1) increased, and the T_1-weighted MR images became brighter as a result of the enhanced T_1 shortening effect, which is in agreement with the previous results.[5a] In particular, the 3 nm-sized nanocrystals exhibited the highest relaxivity (r_1) of 2.38 $mM^{-1}s^{-1}$. The specific relaxivity measurements of water dispersions of the tetrahedral Mn_3O_4 nanocrystals with edge lengths of 6, 8, and 20 nm were also carried out. As shown in Figure 6b, the tetrahedral Mn_3O_4 nanocrystals exhibited size-dependent MR properties similar to those of the spherical nanocrystals. The r_1 values of spherical manganese oxide nanocrystals are larger than those of tetrahedral nanocrystals with the same volume. According to a review article by S. Laurent and co-workers, the relaxation mechanism is based on paramagnetic systems contributed by either inner- or outer-sphere relaxations.[7g] Inner-sphere relaxation deals with the direct exchange of energy between protons and electrons that are located in the first hydration sphere of the paramagnetic ion and is dominated by dipolar and scalar coupling of the spins. On the other hand, outer-sphere relaxation is due to the movement of the water protons near the local magnetic field gradients generated by the paramagnetic ion. In order to enhance the inner-sphere relaxation, water molecules should be attached to the surface of nanocrystals. In our study, the PEG-phospholipid-capped manganese oxide nanocrystal has no direct contact with water, as there is an inner hydrophobic layer of oleic acid and surfactant on the manganese oxide nanocrystal. In this context, we speculate that an interaction between the proton spins of water and the magnetic moment of paramagnetic Mn^{2+} ions on the nanocrystal surface can be the main dipolar interaction that generates relaxation properties. In addition, as explained by Baek and co-workers, a manganese oxide nanocrystal has a mag-

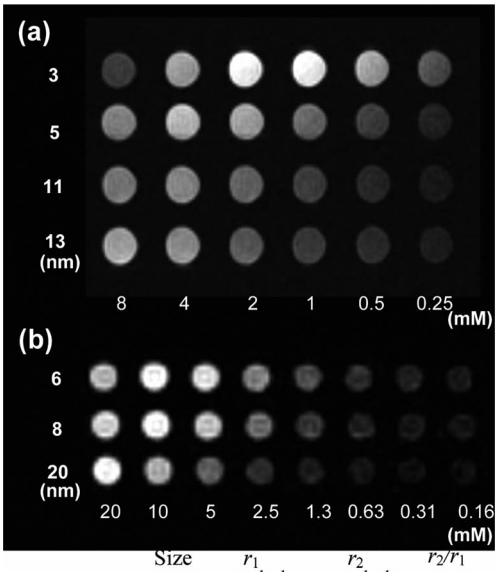

	Size (nm)	r_1 ($mM^{-1}s^{-1}$)	r_2 ($mM^{-1}s^{-1}$)	r_2/r_1
(a) Diameters of the spherical Mn_3O_4 nanoparticles	3	2.38	7.27	3.05
	5	1.39	3.66	2.63
	11	0.99	2.84	2.87
	13	0.41	1.26	3.07
(b) Edge lengths of the tetrahedral Mn_3O_4 nanoparticles	6	1.08	1.36	1.26
	8	0.63	1.19	1.89
	20	0.25	0.44	1.76

Figure 6. Size-dependent T_1-weighted magnetic resonance images and specific relaxivities of (a) spherical and (b) tetrahedral Mn_3O_4 nanocrystals at various Mn^{2+} ion concentrations in water.

netic moment due to incomplete cancelation of the antiferromagnetic spins in an oxide lattice.[9d] The Mn^{2+} ions on the surface of nanocrystals can increase the magnetic moment by breaking the symmetry of an oxide lattice. The high surface-to-volume ratio of small nanocrystals causes a higher contrast effect through enhanced relaxation caused by the surface Mn^{2+} ions. The magnetic-resonance-active Mn^{2+} ions on the surface of the Mn_3O_4 nanocrystals shorten the T_1 relaxation time of water protons, thus rendering brighter MR images.

Conclusions

In summary, we report the size- and shape-controlled synthesis of manganese oxide nanocrystals by the thermal decomposition of a Mn–oleate complex through a heat-up process. When the thermal decomposition of the Mn^{II}–oleate complex was conducted in non-coordinating hydrocarbon solvents, uniformly sized MnO nanocrystals with cubic and octahedral shapes were synthesized. When the thermal decomposition was performed in the presence of strongly coordinating carboxylic acid surfactants, spherical nanocrystals were generated, whose diameters were controlled from 3 to 13 nm by varying the chain length of the carboxylic acids. Tetrahedral MnO nanocrystals were synthesized by the addition of oleyl alcohol to the reaction mixture at high temperatures. The as-synthesized MnO nanocrystals were transformed to Mn_3O_4 or MnO/Mn_3O_4 core–shell structures by oxidation in air. The air-oxidized MnO/Mn_3O_4 nanocrystals exhibited exchange coupling with shifted magnetic hysteresis loops. Finally, an investigation of the T_1 relaxation properties of the various manganese oxide nanocrystals was carried out. As the size of the nanocrystals decreased, their specific relaxivities increased, thereby generating brighter MR images. In particular, the spherical 3 nm-sized Mn_3O_4 nanocrystals exhibited a high specific relaxivity (r_1) of 2.38 $mM^{-1}s^{-1}$, which clearly demonstrates their potential use as an efficient T_1 MRI contrast agent. The current study provides valuable information for the development of optimal nanocrystal-based T_1 MRI contrast agents by the fine tuning of the sizes and shapes of manganese oxide nanocrystals.

Experimental Section

Chemicals: Hexane, ethanol, and acetone were used as received. Manganese(II) chloride tetrahydrate ($MnCl_2{\cdot}4H_2O$, 98%), oleic acid [$CH_3(CH_2)_7CH{=}CH(CH_2)_7COOH$, 90%], stearic acid ($C_{17}H_{35}COOH$, 95%), myristic acid ($C_{13}H_{27}COOH$, 99%), decanoic acid ($C_9H_{19}COOH$, 96%), and 1-octadecene [$CH_2{=}CH(CH_2)_{15}CH_3$, 90%] were purchased from Aldrich Chemicals. Sodium oleate [$CH_3(CH_2)_7CH{=}CH(CH_2)_7COONa$, 95%], 1-hexadecene [$CH_2{=}CH(CH_2)_{13}CH_3$, 95%], oleyl alcohol [$CH_3(CH_2)_7CH{=}CH(CH_2)_8OH$, 60%], phenyl ether ($C_6H_5OC_6H_5$, 99%), and trimethylamine *N*-oxide [$(CH_3)_3NO$, 98%] were purchased from TCI Organic Chemicals. Behenic acid ($C_{21}H_{43}COOH$) was purchased from Kanto Chemicals. 1,2-distearoyl-*sn-glycero*-3-phosphoethanolamine-*N*-[methoxy-(polyethylene glycol)-2000] (mPEG-2000 PE) was purchased from Avanti Polar Lipids, Inc.

Synthesis of Mn^{II}–Oleate Complex: The Mn^{II}–oleate complex was prepared by reacting manganese chloride with sodium oleate. In a typical synthesis, manganese chloride ($MnCl_2{\cdot}4H_2O$, 7.92 g, 40 mmol, Aldrich, 98%) and sodium oleate (24.36 g, 80 mmol, TCI, 95%) were dissolved in a solvent mixture composed of ethanol (40 mL), distilled water (30 mL), and hexane (70 mL). The resulting solution was heated to 60 °C and kept at this temperature for 4 h. It was then transferred to a separatory funnel, and the upper hexane layer containing the Mn–oleate complex was collected and washed several times with distilled water. Evaporation of hexane afforded the Mn^{II}–oleate complex. When the Mn–oleate complex adsorbed water in air, its appearance changed from a pink powder to a red-brown solid (Supporting Information, Figure S1). Therefore, the collection of the hexane layer and the evaporation should be conducted promptly to get Mn–oleate as pink powder. In addition, the Mn^{II}–oleate powder should be stored in a desiccator or in a dry box before use.

Synthesis of MnO Nanocrystals with Cubic, Octahedral, and Spherical Shapes

For all of the experiments described here regarding the synthesis of manganese oxide nanocrystals, standard Schlenk techniques were used. The solution containing Mn^{II}–oleate, surfactants, and solvents was degassed at 70 °C for 1 h under vacuum to remove water and oxygen prior to the synthesis. The resulting mixture was then heated to high temperatures with vigorous stirring under an argon atmosphere. In a typical synthesis of MnO nanocubes of size 16 nm, Mn oleate (1.24 g, 2 mmol) was dissolved in 1-hexadecene (10 g) at room temperature. The reaction mixture was degassed, then heated to reflux (ca. 288 °C) at a rate of 2 °C min^{-1} with vigorous stirring under an argon atmosphere, and kept at this temperature for 1 h. The color of the solution gradually changed from pink to deep green. The solution was then cooled to room temperature, and hexane (20 mL) was added to the solution, followed by the addition of acetone (80 mL) to precipitate the MnO nanocrystals. The waxy precipitate was retrieved by centrifugation. When the reaction was conducted in 1-octadecene instead of 1-hexadecene at 320 °C for 30 min and all the other synthetic conditions were kept unchanged, octahedral MnO nanocrystals with an average edge length of 26 nm were produced. When the reaction was performed in 1-octadecene at the same temperature for 1 h, MnO nanocrystals of size 29 nm were generated. The as-synthesized nanocrystals were washed with acetone several times to remove excess surfactant and then dispersed in chloroform.

When we performed the synthesis in 1-hexadecene in the presence of a carboxylic acid surfactant, spherical MnO nanocrystals were produced. When a reaction mixture composed of Mn^{II} oleate (1.24 g, 2 mmol), 1-hexadecene (10 g), and carboxylic acid (2 mmol) was heated to reflux (ca. 288 °C) at a rate of 5 °C min^{-1} with vigorous stirring under an argon atmosphere and kept at this temperature for 2 h, spherical MnO nanocrystals with diameters of 3, 5, 11, and 13 nm were generated, when the carboxylic acid used was behenic, stearic, myristic, and decanoic acid, respectively.

Synthesis of MnO Nanorods: In a typical synthesis of the rod-shaped MnO nanocrystals, myristic acid or decanoic acid (2 mmol) was added to a solution of Mn^{II} oleate (1.24 g) in 1-hexadecene (10 g). The resulting mixture was then heated to 280 °C at a rate of 2 °C min^{-1} with vigorous stirring under an argon atmosphere and kept at this temperature for 2 h. After cooling to room temperature, rod-shaped MnO nanocrystals were obtained.

Synthesis of Tetrahedral MnO Nanocrystals: In a typical synthesis of tetrahedral MnO nanocrystals, Mn oleate (1.24 g) was dissolved in phenyl ether (10 g), and the solution was heated up to 260 °C at a rate of 2 °C min^{-1} under an argon atmosphere. Then, oleyl alcohol (4 mL) was added to the solution by using a glass syringe, and the color of the solution gradually changed from pale pink to deep green. After cooling to room temperature, tetrahedral nanocrystals with edge lengths of 6, 8, and 20 nm were obtained by variation of the heating rate and reaction time (Table S1 in the Supporting Information).

Synthesis of Mn_3O_4 Nanocrystals from MnO Nanocrystals: As-synthesized MnO nanocrystals were gradually oxidized to MnO/Mn_3O_4 core–shell structures or Mn_3O_4 under ambient conditions. For an intentional oxidation of MnO nanocrystals, MnO nanocrystal powder (0.1 g) was added to 1-octadecene (10 g) in the presence of dried trimethylamine *N*-oxide (0.45 g, 6 mmol) at room temperature, and the mixture was degassed at 70 °C for 1 h under vacuum. It was then heated to 300 °C with vigorous stirring and kept at this temperature for 2 h.

Characterization of the Materials: The manganese oxide nanocrystals were characterized by low- and high-resolution transmission electron microscopy (TEM and HRTEM), electron diffraction (ED), X-ray diffraction (XRD), and superconducting quantum interference device (SQUID) magnetometry. The TEM images were obtained with a JEOL 2010 microscope operated at 200 kV. Powder XRD was performed with a Rigaku D/Max-3C diffractometer (Cu-K_α radiation, λ = 0.15418 nm). The magnetic properties were investigated with zero-field-cooling (ZFC) and field-cooling (FC) procedures in an applied magnetic field of 100 Oe between 5 and 300 K, and hysteresis loops were measured at 5 K with a commercial SQUID magnetometer (Quantum Design, MPMS5XL).

Magnetic Resonance (MR) Relaxivity Measurements: Water-dispersible and biocompatible manganese oxide nanocrystals were prepared by a previously reported method with some modifications. In a typical procedure, mPEG-2000 PE (20 mg) in chloroform (2 mL) was added to manganese oxide nanocrystals (10 mg) dispersed in of chloroform (1 mL). After evaporating the chloroform, the residue was incubated at 60 °C in vacuum for 1 h. When water (10 mL) was added to the residue, a clear brown suspension was generated. After filtration (0.2 μm syringe filter, cellulose acetate), excess mPEG-2000 PE was removed by ultracentrifugation (40000 rpm, 1 h, 2 times). When the as-synthesized MnO nanocrystals were transferred into water in the presence of mPEG-2000 PE, the nanocrystals were further oxidized to Mn_3O_4 nanocrystals. The PEG-phospholipid-capped nanocrystals exhibit high colloidal stability and no sign of aggregation (for details, see Supporting Information, Figure S2). The T_1 and T_2 relaxation times of the Mn_3O_4 nanocrystals dispersed in water were measured with a 1.5 T clinical MRI scanner (GE Signa Excite) at various Mn^{2+} ion concentrations. The Mn^{2+} ion concentration was determined by inductively coupled plasma atomic emission spectroscopy (ICP-AES) after all the nanocrystals were completely etched in hydrochloric acid. An inversion-recovery fast spin-echo (IR-FSE) sequence with 30 inversion time (TI) values [relaxation time (TR): 4400 ms, echo time (TE): 8.4 ms, TI: 50–4000 ms] for the T_1 measurement and a conventional Carr–Purcell–Meiboom–Gill (CPMG) sequence with 12 TE values (TR: 5000 ms, TE: 16–200 ms) for the T_2 measurement were performed with a head coil on a 1.5 T MRI scanner. The T_1 and T_2 relaxation times were calculated by fitting the variation of the signal intensity with the TE or TI values by using a monoexponential function, namely, $|[1 - (1 - k)\exp(-TI/T_1)]M_0|$, by means of a nonlinear least-squares fit and by utilizing the Levenberg–Marquardt algorithm.

Supporting Information (see footnote on the first page of this article): Photographs of pink and brown Mn–oleate complexes; size distribution histograms, XRD patterns, TEM images, magnetic parameters, and details of the syntheses of manganese oxide nanocrystals.

Acknowledgments

T. H. acknowledges financial support by the Korean Ministry of Education, Science and Technology through the Global Research Laboratory (2011-0021628), Strategic Research (2010-0029138), and the World Class University (R31-10013) programs of the National Research Foundation (NRF) of Korea.

[1] a) K. J. Klabunde, *Nanoscale Materials in Chemistry*, Wiley-Interscience, New York, **2001**; b) T. Hyeon, *Chem. Commun.* **2003**, 927; c) S. Sun, *Adv. Mater.* **2006**, *18*, 393; d) Y. Xia, P. Yang, Y. Sun, Y. Wu, B. Mayers, B. Gates, Y. Yin, F. Kim, H. Yan, *Adv. Mater.* **2003**, *15*, 353; e) A.-H. Lu, E. L. Salabas, F. Schüth, *Angew. Chem.* **2007**, *119*, 1242; *Angew. Chem. Int. Ed.* **2007**, *46*, 1222; f) M. Niederberger, G. Garnweitner, *Chem. Eur. J.* **2006**, *12*, 7282.

[2] a) J. Pike, J. Hanson, L. Zhang, S.-W. Chan, *Chem. Mater.* **2007**, *19*, 5609; b) T. D. Schladt, T. Graf, W. Tremel, *Chem. Mater.* **2009**, *21*, 3183; c) Q. Li, J. Wang, Y. He, W. Liu, X. Qiu, *Cryst. Growth Des.* **2009**, *9*, 3100; d) P. Li, C. Nan, Z. Wei, J. Lu, Q. Peng, Y. Li, *Chem. Mater.* **2010**, *22*, 4232; e) N. Wang, X. Cao, L. He, W. Zhang, L. Guo, C. Chen, R. Wang, S. Yang, *J. Phys. Chem. C* **2008**, *112*, 365.

[3] a) G. Salazar-Alvarez, J. Sort, S. Suriñach, M. D. Baró, J. Nogués, *J. Am. Chem. Soc.* **2007**, *129*, 9102; b) A. E. Berkowitz, G. F. Rodriguez, J. I. Hong, K. An, T. Hyeon, N. Agarwal, D. J. Smith, E. E. Fullerton, *Phys. Rev. B* **2008**, *77*, 024403; c) A. López-Ortega, D. Tobia, E. Winkler, I. V. Golosovsky, G. Salazar-Alvarez, S. Estradé, M. Estrader, J. Sort, M. A. González, S. Suriñach, J. Arbiol, F. Peiró, R. D. Zysler, M. D. Baró, J. Nogués, *J. Am. Chem. Soc.* **2010**, *132*, 9398.

[4] a) M. Yin, S. O'Brien, *J. Am. Chem. Soc.* **2003**, *125*, 10180; b) M. A. Morales, R. Skomski, S. Fritz, G. Shelburne, J. E. Shield, M. Yin, S. O'Brien, D. L. Leslie-Pelecky, *Phys. Rev. B* **2007**, *75*, 134423; c) W. S. Seo, H. H. Jo, K. Lee, B. Kim, S. J. Oh, J. T. Park, *Angew. Chem.* **2004**, *116*, 1135; *Angew. Chem. Int. Ed.* **2004**, *43*, 1115; d) J. Park, E. Kang, C. J. Bae, J.-G. Park, H.-J. Noh, J.-Y. Kim, J.-H. Park, H. M. Park, T. Hyeon, *J. Phys. Chem. B* **2004**, *108*, 13594; e) Y.-P. Du, Y.-W. Zhang, L.-D. Sun, C.-H. Yan, *J. Phys. Chem. C* **2009**, *113*, 6521; f) I. Djerdj, D. Arćon, Z. Jagličić, M. Niederberger, *J. Phys. Chem. C* **2007**, *111*, 3614; g) G. H. Lee, S. H. Huh, J. W. Jeong, B. J. Choi, S. H. Kim, H.-C. Ri, *J. Am. Chem. Soc.* **2002**, *124*, 12094; h) N. Wang, L. Gao, L. He, X. Cao, C. Chen, R. Wang, S. Yang, *Small* **2007**, *3*, 606; i) N. Zhao, W. Nie, X. Liu, S. Tian, Y. Zhang, X. Ji, *Small* **2008**, *4*, 77; j) Y. Tan, L. Meng, Q. Peng, Y. Li, *Chem. Commun.* **2011**, *47*, 1172.

[5] a) J. Park, K. An, Y. Hwang, J.-G. Park, H.-J. Noh, J.-Y. Kim, J.-H. Park, N.-M. Hwang, T. Hyeon, *Nat. Mater.* **2004**, *3*, 891; b) S. G. Kwon, Y. Piao, J. Park, S. Anagappane, Y. Jo, N.-M. Hwang, J.-G. Park, T. Hyeon, *J. Am. Chem. Soc.* **2007**, *129*, 12571.

[6] I. Rusakova, T. Ould-Ely, C. Hofmann, D. Prieto-Centurion, A. Kumar, C. S. Lavin, N. J. Halas, A. Lüttge, K. H. Whitemire, *Chem. Mater.* **2007**, *19*, 1369.

[7] a) J.-H. Lee, Y.-M. Huh, Y.-w. Jun, J.-w. Seo, J.-t. Jang, H.-T. Song, S. Kim, E.-J. Cho, H.-G. Yoon, J.-S. Suh, J. Cheon, *Nat. Med.* **2007**, *13*, 95; b) Y.-w. Jun, J.-w. Seo, J. Cheon, *Acc. Chem. Res.* **2008**, *41*, 179; c) R. Weissleder, K. Kelly, E. Y. Sun, T. Shtatland, L. Josephson, *Nat. Biotechnol.* **2005**, *23*, 1418; d) J. W. M. Bulte, D. L. Kraitchman, *NMR Biomed.* **2004**, *17*, 484; e) H. Gu, K. Xu, C. Xu, B. Xu, *Chem. Commun.* **2006**, 941; f)

J. Y. Park, E. S. Choi, M. J. Baek, G. H. Lee, S. Woo, Y. Chang, *Eur. J. Inorg. Chem.* **2009**, 2477; g) S. Laurent, D. Forge, M. Port, A. Roch, C. Robic, L. V. Elst, R. N. Muller, *Chem. Rev.* **2008**, *108*, 2064.

[8] a) H. B. Na, J. H. Lee, K. An, Y. I. Park, M. Park, I. S. Lee, D.-H. Nam, S. T. Kim, S.-H. Kim, S.-W. Kim, K.-H. Lim, K.-S. Kim, S.-O. Kim, T. Hyeon, *Angew. Chem.* **2007**, *119*, 5493; *Angew. Chem. Int. Ed.* **2007**, *46*, 5397; b) H. B. Na, I. C. Song, T. Hyeon, *Adv. Mater.* **2009**, *21*, 2133.

[9] a) J. Shin, R. M. Anisur, M. K. Ko, G. H. Im, J. H. Lee, I. S. Lee, *Angew. Chem.* **2009**, *121*, 327; *Angew. Chem. Int. Ed.* **2009**, *48*, 321; b) D. Choi, A. Han, J. P. Park, J. K. Kim, J. H. Lee, T. H. Kim, S.-W. Kim, *Small* **2009**, *5*, 571; c) E. S. Choi, J. Y. Park, M. J. Baek, W. Xu, K. Kattel, J. H. Kim, J. J. Lee, Y. Chang, T. J. Kim, J. E. Bae, K. S. Chae, K. J. Seo, G. H. Lee, *Eur. J. Inorg. Chem.* **2010**, 4555; d) M. J. Baek, J. Y. Park, W. Xu, K. Kattel, H. G. Kim, E. J. Lee, A. K. Patel, J. J. Lee, Y. Chang, T. J. Kim, J. E. Bae, K. S. Chae, G. H. Lee, *ACS Appl. Mater. Interfaces* **2010**, *2*, 2949; e) C.-C. Huang, N.-H. Khu, C.-S. Yeh, *Biomaterials* **2010**, *31*, 4073.

[10] J. Pike, J. Hanson, L. Zhang, S.-W. Chan, *Chem. Mater.* **2007**, *19*, 5609.

[11] a) A. Puglisi, S. Mondini, S. Cenedese, A. M. Ferretti, N. Santo, A. Ponti, *Chem. Mater.* **2010**, *22*, 2804; b) R. Zheng, H. Gu, B. Xu, K. K. Fung, X. Zhang, S. P. Ringer, *Adv. Mater.* **2006**, *18*, 2418; c) S. Xie, X. Zhou, X. Han, Q. Huang, M. Jin, Y. Jiang, Z. Xie, L. Zheng, *J. Phys. Chem. C* **2009**, *113*, 19107; d) Z. Quan, J. Fang, *Nano Today* **2010**, *5*, 390.

[12] a) T. Sugimoto, *Monodispersed Particles*, Elsevier, New York, **2001**; b) J. Cheon, M.-J. Kang, S.-M. Lee, J.-H. Lee, J.-H. Yoon, S. J. Oh, *J. Am. Chem. Soc.* **2004**, *126*, 1950; c) D. Kim, N. Lee, M. Park, B. H. Kim, K. An, T. Hyeon, *J. Am. Chem. Soc.* **2009**, *131*, 454; d) P. Guardia, N. Pérez, A. Labarta, X. Batlle, *Langmuir* **2010**, *26*, 5843.

[13] a) M. V. Kovalenko, M. I. Bodnarchuk, R. T. Lechner, G. Hesser, F. Schäffler, W. Heiss, *J. Am. Chem. Soc.* **2007**, *129*, 6352; b) Z. Chen, H. Chen, H. Hu, M. Yu, F. Li, Q. Zhang, Z. Zhou, T. Yi, C. Huang, *J. Am. Chem. Soc.* **2008**, *130*, 3023; c) A. L. Willis, N. J. Turro, S. O'Brien, *Chem. Mater.* **2005**, *17*, 5970; d) N. J. Turro, P. H. Lakshminarasimhan, S. Jockusch, S. P. O'Brien, S. G. Grancharov, F. X. Redl, *Nano Lett.* **2002**, *2*, 325; e) L. Wang, P. Li, J. Zhuang, F. Bai, J. Feng, X. Yan, Y. Li, *Angew. Chem.* **2008**, *120*, 1070; *Angew. Chem. Int. Ed.* **2008**, *47*, 1054; f) Z. L. Wang, *J. Phys. Chem. B* **2000**, *104*, 1153.

[14] Y. Chen, E. Johnson, X. Peng, *J. Am. Chem. Soc.* **2007**, *129*, 10937.

[15] a) Z. Tang, N. A. Kotov, M. Giersig, *Science* **2002**, *297*, 237; b) R. L. Penn, J. F. Banfield, *Science* **1998**, *281*, 969; c) C. Pacholski, A. Kornowski, H. Weller, *Angew. Chem.* **2002**, *114*, 1234; *Angew. Chem. Int. Ed.* **2002**, *41*, 1188; d) J. H. Yu, J. Joo, H. M. Park, S.-I. Baik, Y. W. Kim, S. C. Kim, T. Hyeon, *J. Am. Chem. Soc.* **2005**, *127*, 5662; e) K.-S. Cho, D. V. Talapin, W. G. Gaschler, C. B. Murray, *J. Am. Chem. Soc.* **2005**, *127*, 7140.

[16] a) D. Zitoun, N. Pinna, N. Frolet, C. Belin, *J. Am. Chem. Soc.* **2005**, *127*, 15034; b) X. Zhong, R. Xie, L. Sun, I. Lieberwirth, W. Knoll, *J. Phys. Chem. B* **2006**, *110*, 2; c) T. Ould-Ely, D. Prieto-Centurion, A. Kumar, W. Guo, W. V. Knowles, S. Asokan, M. S. Wong, I. Rusakova, A. Lüttge, K. H. Whitemire, *Chem. Mater.* **2006**, *18*, 1821.

[17] Y. Chen, M. Kim, G. Lian, M. B. Johnson, X. Peng, *J. Am. Chem. Soc.* **2005**, *127*, 13331.

[18] a) P. Guardia, B. Batelle-Brugal, A. G. Roca, O. Iglesias, M. P. Morales, C. J. Serna, A. Labarta, X. Batlle, *J. Magn. Magn. Mater.* **2007**, *316*, e756; b) G. F. Goya, T. S. Berquó, F. C. Fonseca, M. P. Morales, *J. Appl. Phys.* **2003**, *94*, 3520.

[19] a) W. H. Meiklejohn, C. P. Bean, *Phys. Rev.* **1956**, *102*, 1413; b) J. Nogués, I. K. Schuller, *J. Magn. Magn. Mater.* **1999**, *192*, 203; c) V. Skumryev, S. Stoyanov, Y. Zhang, G. Hadjipanayis, D. Divord, J. Nogués, *Nature* **2003**, *423*, 850.

[20] P. Petracic, Z.-P. Li, I. V. Roshchin, M. Viret, R. Morales, X. Batlle, I. K. Schuller, *Appl. Phys. Lett.* **2005**, *87*, 222509.

[21] T. Yu, J. Moon, J. Park, Y. I. Park, H. B. Na, B. H. Kim, I. C. Song, W. K. Moon, T. Hyeon, *Chem. Mater.* **2009**, *21*, 2272.

Received: October 27, 2011
Published Online: February 10, 2012

